Journal of Oleo Science
Copyright ©2024 by Japan Oil Chemists' Society
J-STAGE Advance Publication date : March 25, 2024
doi : 10.5650/jos.ess23208
J. Oleo Sci.

Synthesis of *Ottonia anisum* Extract Mediated ZnO NPs and Their Local Anesthetic, Analgesic and HCl-induced Acute Lung Injury Activities

Guiqin Fan[#], Jing Yu[#], Zhengzheng Tao, Xingjia Qian, Qinghong Qian, Jun Shu, Dongfang Shi, Luhong Shen, Bing Lu[*], and Hong Lv[*]

Department of Pulmonary and Critical Care Medicine, Taicang Hospital of Traditional Chinese Medicine, Taicang TCM Hospital Affiliated to Nanjing University of Chinese Medicine, Suzhou 215400, Jiangsu, CHINA

Abstract: In this study, we outlined the green synthesis of Zinc oxide nanoparticles (ZnO NPs) using the plant-mediated method. Employing the nitrate derivative of Zinc and the extract from the native medicinal plant, *Ottonia anisum*, the nanoparticles were effectively produced. After obtaining a yellow-colored paste, it was meticulously dried, gathered, and set aside for subsequent examination. The UV-visible spectrometry analysis indicated an absorption peak at 320 nm, which is indicative of ZnO NPs. Characterization techniques, such as XRD and HR-TEM, confirmed the existence of agglomerated ZnO NPs with an average diameter of 40 nm. Through EDS analysis, distinct energy signals for both Zinc and Oxygen were observed, confirming their composition. Furthermore, FT-IR spectroscopy highlighted an absorption peak for Zn–O bonding in the range of 400 to 600 cm^{-1}. Further, we employed three distinct pain models in mice to evaluate the influence of ZnO NPs on the nociceptive threshold. Our findings revealed that, when orally administered, ZnO NPs at concentrations ranging from 5-20 mg/kg exerted a dose-dependent analgesic effect in both the hot-plate and the acetic acid-induced writhing tests. Moreover, when ZnO NPs were administered at doses between 2.5-10 mg/kg, there was a notable reduction in pain responses during both the initial and subsequent phases of the formalin test, but no change in PGE_2 production within the mice's hind paw was found. On the other hand, acute lung injury studies revealed that the administration of ZnO NPs orally 90 minutes prior to HCl instillation decreased the neutrophil infiltration into the lungs in a dose-responsive manner. This reduction in pulmonary inflammation was paralleled by a significant decrease in lung edema, as evidenced by the reduced total protein content in the BALF. Additionally, the ZnO NPs appeared to recalibrate the lung's redox equilibrium following HCl exposure, which was determined through measurements of ROS, malondialdehyde, glutathione, and catalase activity. All these results further indicated the potential of biofabricated ZnO NPs for future applications in analgesics and acute lung injury treatments.

Key words: ZnO NPs, acute lung injury, analgesic, plant extract

1 Introduction

Nanotechnology is recently considered as a progressive technology with diverse applications spanning various sectors, including the pharmaceutical, food, mechanical, and chemical industries. This technology finds intriguing uses in areas like computing, energy production, environmental, drug delivery, optics, and medical science[1)]. With the emergence of nanoscience, a variety of nanoscale devices have been introduced via diverse methodologies, including physical, chemical, and eco-friendly processes. Among these, the green synthesis of nanoparticles is especially favored due to its ease and adaptability[2)]. On the other hand, the traditional nanoparticle synthesis methods have their limitations, such as prolonged processing times, elevated costs, complex procedures, and the involvement of hazardous chemicals. Consequently, research has pivoted towards more sustainable and efficient synthesis protocols for nanoparticle production[3, 4)]. For researchers in materials science, pioneering green technologies for the creation of nanomaterials has become a priority. In this

[#] Co-First Author
[*]Correspondence to: Bing Lu, Department of Pulmonary and Critical Care Medicine, Taicang Hospital of Traditional Chinese Medicine, Taicang TCM Hospital Affiliated to Nanjing University of Chinese Medicine, Suzhou 215400, Jiangsu, CHINA. Hong Lv, Department of Pulmonary and Critical Care Medicine, Taicang Hospital of Traditional Chinese Medicine, Taicang TCM Hospital Affiliated to Nanjing University of Chinese Medicine, Suzhou 215400, Jiangsu, CHINA
E-mail: Lubing0@hotmail.com (BL), lovhing@163.com (HL)
Accepted January 3, 2024 (received for review October 9, 2023)
Journal of Oleo Science ISSN 1345-8957 print / ISSN 1347-3352 online
https://www.jstage.jst.go.jp/browse/jos/ https://mc.manuscriptcentral.com/jjocs

context, the biosynthesis of nanomaterials, particularly leveraging plant extracts, has emerged as a preferred method in green chemistry because of its simplicity, cost-effectiveness, and non-toxic nature[5–7]. Moreover, nanotechnology has positively influenced various facets of human life, addressing challenges ranging from energy sustainability and climate change to innovations in beauty, textiles, and healthcare, even offering potential treatments for severe illnesses like cancer and Alzheimer's disease[8, 9].

Recently, there is a heightened interest in exploring metal oxide nanoparticles due to their versatile applications across multiple technological domains[10]. Specifically, ZnO NPs have emerged as promising inorganic entities given their myriad of benefits. These nanoparticles find applications in diverse areas such as chemical sensors, cosmetics, electronics, textiles, semiconductors, energy conservation, catalysis, and healthcare[11–15]. Furthermore, ZnO NPs are lauded for their non-toxicity and biocompatibility, making them suitable for various biomedical uses, including but not limited to anticancer treatments[16], anti-inflammatory therapies[17], antibacterial, targeted drug delivery[18] and bioimaging[19, 20].

On the other hand, the partial effectiveness of existing pharmacological treatments emphasizes the necessity to innovate and introduce novel agents to address ALI. The burgeoning field of nanomedicine provides potential insights into this challenge. These nanomedical solutions, with their capability for either active or passive targeting, have demonstrated therapeutic benefits in diverse medical conditions. For instance, the nano-encapsulation of dexamethasone is proposed to enhance its role in managing COVID-19, given its proficiency in targeting overstimulated immune responses and its noted anti-edema properties[21]. Agents like pharmaceuticals, siRNA, and proteins can be integrated or housed within nanomedicine structures[22, 23]. Amid ALI, there's a noted increase in vascular permeability, coupled with changes in oxidants, pH levels, enzymes, and the microenvironment, as well as shifts in cell surface receptor expressions[24]. These physiological alterations can be exploited for precision delivery and controlled drug release. Consequently, ALI-focused nanomedicine presents a spectrum of therapeutic avenues ranging from site-specific anti-inflammatory agent delivery[25, 26], to neutralizing inflammatory agents directly[27–30], modulating activities of inflammatory cells[31–33]and intervening in inflammatory signaling processes[34–36]. Different nanomedicine tools operate on various cellular or pathophysiological mechanisms, with several showing promising outcomes both in lab and clinical settings.

While nanoparticles can be synthesized through multiple methods, each yielding product with unique properties and extensive applications, green technologies for production of ZnO NPs has been explored. However, there's a noticeable gap in the literature regarding their varied biological attributes, encompassing antimicrobial, antilarvicidal, protein kinase inhibition, analgesic, acute lung injury treatments and anticancer activities. In this work, ZnO NPs were prepared using *Ottonia anisum* leaf extract as reducing agent and characterized. The prepared ZnO NPs were studied for their analgesic effect and acute lung injury treatment in mice.

2 Experiments

2.1 Materials

Bovine serum albumin(BSA), Potassium bromide(KBr), 2'7'-dichlorofluorescein diacetate(DCF-DA), $Zn(NO_3)_2.6H_2O$, formalin, Acetic acid and other chemicals were purchased from Sigma Aldrich, Shanghai.

2.2 *Ottonia anisum* extract preparation

The *Ottonia anisum* plant leaves were first rinsed meticulously using distilled water to eliminate any dust or foreign contaminants. Post washing, these leaves were left to air-dry at ambient temperature. A total of 50 g of the dried leaves were taken for the subsequent procedures. These leaves were then finely chopped and pulverized with a mortar and pestle, with an adequate amount of water added for efficient grinding to prepare concentrations consisting of 25 g in 50 mL. This crude extract was then subjected to a boiling process for about 15 minutes, which aids in softening the cellular membranes. Following this, the boiled extract was filtered utilizing Cellulose nitrate filter paper. To separate any residual particulate matter, the filtrate was then centrifuged at a speed of 3000 rpm for a duration of 10 min. The resulting clear supernatant was preserved for subsequent analysis and experiments.

2.3 Preparation of ZnO NPs

About 5 mL of 10 mM solution of $Zn(NO_3)_2.6H_2O$ was combined with 10 mL of the prepared *Ottonia anisum* leaf extract. The resulting mixture underwent stirring at 65℃ for a duration of 20 min. Following this process, a light-yellow transformation of the reaction mixture was observed. This mixture was then permitted to remain heated overnight at a consistent temperature, culminating in the formation of a dense yellowish paste. Once formed, this paste underwent a thorough drying process and was subsequently calcined at a temperature of 400℃ for a period of 2 h. After this, the product was carefully gathered and stored separately, readying it for subsequent characterization steps.

2.4 Characterization of ZnO NPs

The absorbance of ZnO NPs were assessed using an Ultraviolet-Visible Spectrometer from the Cary Series by Agilent Technology. Measurements were taken over a

wavelength spectrum ranging from 200 nm to 800 nm. ZnO aqueous dispersion was used for UV-visible spectral analysis. The nanoparticle size and crystalline phases were ascertained using X-ray diffraction (XRD). The analysis employed the EMPYREAN diffractometer, which scattered Cu Kα radiation with a wavelength of 0.154 nm. Measurements were taken across a 2θ range spanning from 20 to 80℃, operating the instrument at 45 kV and 40 mA. Images of the ZnO nanoparticles (NPs) were obtained using a Hi-resolution Transmission Electron Microscope (HR-TEM; model JEM 2010 from JEOL, Japan). To prepare the sample for TEM imaging, Aqueous ZnO NPs dispersion were carefully placed onto a carbon-coated copper grid and was left to dry at ambient temperature for approximately 3 hours before commencing the TEM examination. The same instrument was used for energy-dispersive X-ray spectroscopy (EDS) analysis. The ZnO nanoparticles (NPs) were characterized for their functional groups using Fourier Transform Infrared Spectroscopy (FTIR; model FTIR 8400S, Shimadzu, Japan). To prepare the sample for FTIR analysis, 2 mg of NPs were uniformly blended with 200 mg of potassium bromide and then compacted to create a consistent sample pellet. The spectral transmittance of the sample was recorded across a wavenumber range of 500 to 4000 cm^{-1} at a resolution of 4 cm^{-1}.

2.5 Local anesthetic activity

Wistar rats, either male or female, weighing between 100-150 g and aged one month, along with female Kunming mice weighing 20-25 g, were used in this experiment. These animals were kept under a consistent temperature of approximately 22℃ and subjected to a 12-h light/dark cycle. They were given unrestricted access to both water and food. However, for 12 h leading up to any experiment, they were only provided with water to ensure that food did not interfere with the absorption of tested substances. Mice were given ZnO NPs orally at doses ranging from 1-20 mg/kg. For comparison, control mice were orally administered an equivalent amount of normal saline (20 mL/kg). Additionally, some mice, serving as positive controls, were given either morphine (5 mg/kg) or aspirin (200 mg/kg) orally.

2.5.1 Hot-plate test

Mice were individually positioned on a heated platform set at approximately 55℃. The moment they began to lick their hind paws or attempted to leap out was noted as the initial reaction time. To prevent any harm to the mice, a limit of 60 sec was set. Before introducing any drug, an initial reaction time was established. Any mouse displaying a reaction time of below 5 sec or higher than 30 sec was ignored from the examination. The reaction time for pulling away the paw was evaluated 30 min post-drug delivery. The effectiveness of the drug, termed the maximum possible effect (MPE), was derived using the formula:

$$MPE\% = [(\text{reaction time post-drug} - \text{initial reaction time})/(60 - \text{initial reaction time})] \times 100$$

2.5.2 Acetic acid induced writhing response

Thirty minutes following the drug's administration, mice were intraperitoneally injected with a 0.6% acetic acid saline solution at a dosage of 10 mL/kg. Following this, each mouse was placed in individual observation chambers. Over the next 20 min, we recorded instances of writhing behaviour, characterized by abdominal muscle contractions accompanied by hind limb stretching.

2.5.3 Formalin induced Hind paw licking response

Thirty minutes after administering the drug, formalin test was performed. Succinctly, micro syringe was used to inject 25 μL of 1.4% formalin (equivalent to 0.5% formaldehyde) just beneath the right hind paw's surface. The duration during which the mouse licked the injected area was timed as a marker of discomfort. Two distinct phases were observed: the early phase considering 0-5 min, representing neurogenic pain and the later phase of 15-30 min, indicative of inflammatory pain responses. Upon completion, the mice were euthanized. Both hind paws were then separated, weighed individually, and subsequently finely chopped and homogenized. This mixture underwent centrifugation at 2500 rpm for 10 min, after which the clear supernatant was set aside for PGE_2 and protein analysis.

2.5.4 PGE_2 Measurement

The mouse hind paw tissue was analysed for PGE_2 levels using an ELISA kit, as per guidelines given by the manufacturer. Simultaneously, protein concentrations were evaluated using the Coomassie blue protein-binding assay, with BSA serving as the reference.

2.6 Acute lung injury studies

Female mice, aged between 6-8 weeks and weighing between 25-30 g, were used for this experiment. They were housed in polypropylene cages and provided with a balanced diet and consistent access to water. Throughout the experimental phase, meticulous care was taken in handling the animals, adhering strictly to the protocols set forth by the University Ethics Committee. Mice were categorized randomly into three distinct groups, each receiving the following treatments:

Group 1 (Control): Mice were provided with standard diet and were not given any other treatment.

Group 2 (ALI): Under anaesthesia, each mouse received an intratracheal administration of 60 μL of 0.1N HCl to simulate acid aspiration-induced ALI.

Group 3 (ALI + ZnO NPs): Mice were segregated into various subgroups. Each subgroup was orally administered ZnO NPs in dosages of either 50, 100, or 200 mg/kg body weight, approximately 90 minutes prior to the HCl introduction.

Each group's treatment was carefully administered, ensuring consistency and accuracy to obtain reliable results.

2.6.1 Assay of biochemical parameters

The protein content in the samples was determined using the Lowry method[37]. ROS levels in lung tissues were ascertained using the DCF-DA dye. To elaborate, Lung tissues, obtained fresh, were used to prepare homogenates. These homogenates underwent incubation in a reaction buffer that contained 10 μM DCF-DA and 10 μM sodium succinate, and this was done for 30 min at 37℃. The ROS in the samples oxidized the DCF-DA into 2,7-dichlorofluorescin, a compound with strong fluorescence. The fluorescence of this compound was subsequently measured with an excitation of 485 nm and an emission of 530 nm[38]. Malondialdehyde (MDA), indicative of lipid peroxidation, was determined using the method set by Ohkawa *et al.* in 1979[39]. Both total and reduced forms of GSH were quantified as per protocols developed by Cleland and Ellman, respectively[40, 41]. Lastly, the activity of catalase in the samples was gauged using the method prescribed by Aebi[42].

3 Results and Discussion

3.1 Characterization

Plants contain secondary metabolites that have the capability to reduce zinc ions in a solution, leading to the formation of ZnO NPs. Not only do these plant extracts function as reducing mediums, but they also serve to stabilize the resultant nanoparticles. The assertion was validated through UV-visible spectral analysis ranging from 280 nm to 800 nm. A distinct optical absorption peak was observed at 320 nm, which aligns with the characteristic spectral signature of ZnO NPs (Fig. 1). Typically, the absorption peak for ZnO NPs is reported to lie between wavelengths of 310 nm and 360 nm[43]. Using the formula $Eg = 1240/\lambda$ eV, the bandgap energy was determined to be 3.8 eV, a value that aligns with previously published data on the energy bandgap of ZnO NPs[44, 45].

The crystallinity of ZnO NPs can be discerned using XRD analysis. The diffractogram displays the intensity of diffracted beams relative to their diffraction angles, revealing insights about the crystalline planes within the sample. Peaks corresponding to the lattice planes such as (100), (002), (101), (102), (110), (103), (112), and (201) were evident in the spectrum were corresponding to the diffraction peaks found at 31.4, 34.1, 36.1, 47.3, 56.3, 62.5, 67.6, 68.8 respectively, as illustrated in Fig. 2. The Scherrer's formula was employed to deduce the average size of these crystalline entities, which was determined to be approximately 52.24 nm. These observed peaks agreed with the standard peaks from the ICDD card with reference number 01-079-0207.

In the transmission electron micrographs (Fig. 3A), ZnO NPs were found agglomerated and nearly spherical in shape with an average diameter of 40 nm. The EDX analysis yielded prominent signals for Zinc and Oxygen, corroborating the existence of Zinc in its oxide state. The characteristic peaks observed for both Zinc and Oxygen further ascertain the synthesis of ZnO NPs. In addition to these primary elements, no other elemental peak was detected indicating the purity of prepared ZnO NPs (Fig. 3B).

The FTIR analysis provides insights into the composition and associated functional groups of the synthesized ZnO NPs. This analysis indicates that the nanoparticle formation results from the interactions among various bioconstituents such as phenolic compounds, alkynes, terpenoids, and flavonoids. As illustrated in Fig. 4, the FTIR spectra of the synthesized ZnO NPs span a range from 400 to 4000 cm^{-1}. These functional groups play a pivotal role in reducing zinc ions to their oxide form, evident from the specific spectral bands. Each identified band is associated with different vibrational modes. A pronounced band at 3275 cm^{-1} can be attributed to the O–H stretching from phenolic compounds. The band at 1624 cm^{-1} signals the presence of

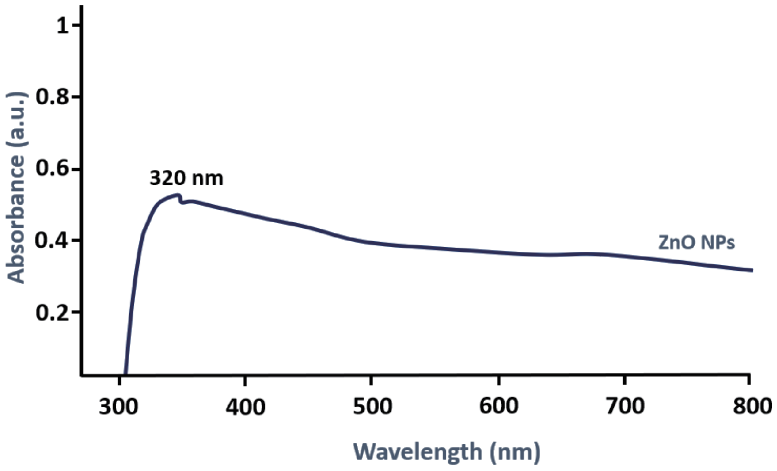

Fig. 1 UV-Visible absorption spectrum of biosynthesized ZnO NPs.

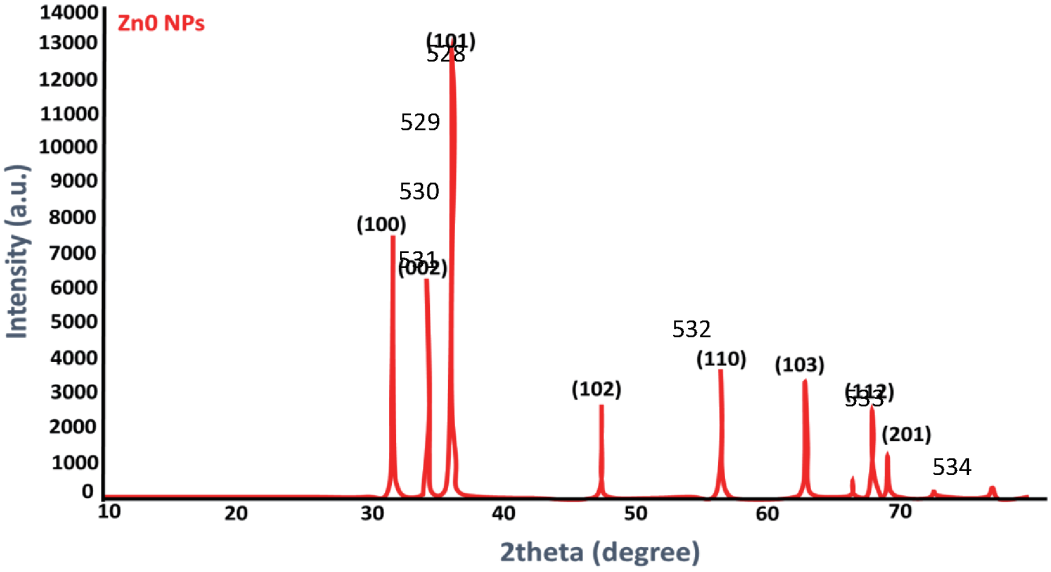

Fig. 2 XRD pattern of biosynthesized ZnO NPs.

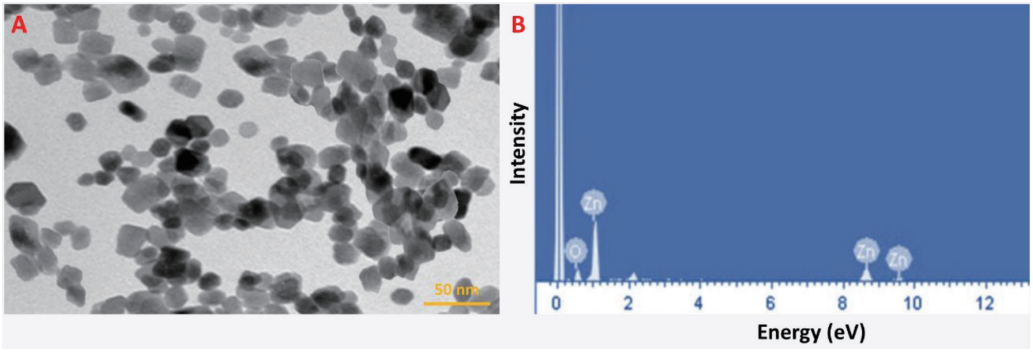

Fig. 3 HR-TEM image (A) and EDS spectrum (B) of prepared ZnO NPs.

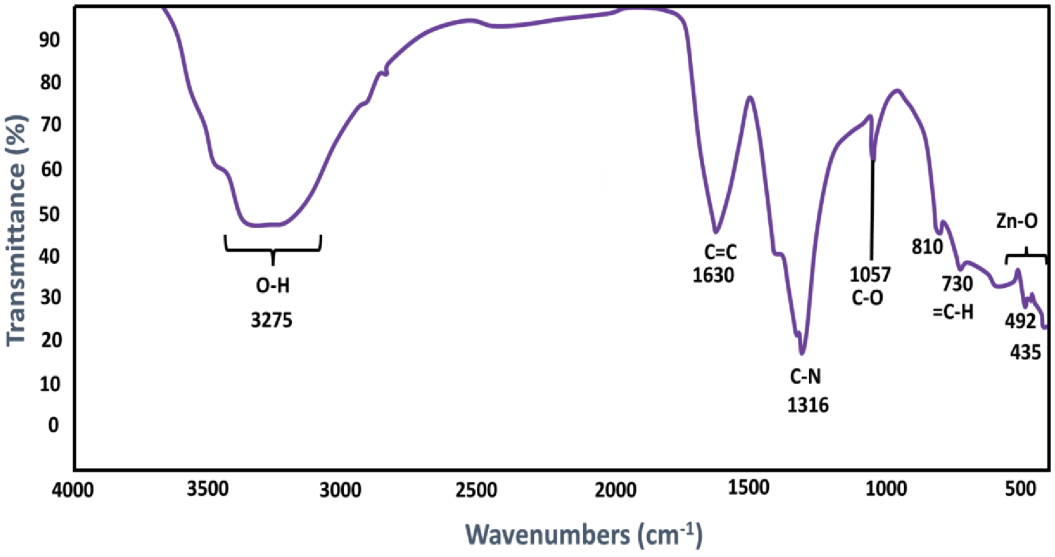

Fig. 4 FTIR spectrum of prepared ZnO NPs.

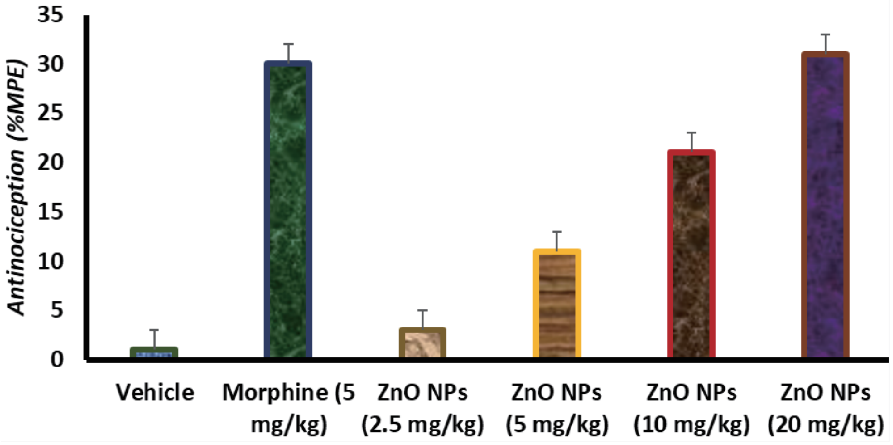

Fig. 5 Hot-plate test showing anti-nociceptive effect of ZnO NPs on mice (n = 8).

Table1 Hot-plate test results showing anti-nociceptive effect of ZnO NPs on in mice.

Groups	Dosage (mg/kg)	Number of withering	% inhibition
Control	–	45.1 ± 6.5	–
Asprin	200	10.8 ± 4.5	73.5
ZnO NPs	20	11.9 ± 5.5	72.8
	10	10.9 ± 5.6	81.4
	5	23.6 ± 5.9	48.0
	2.5	41.4 ± 6.4	13.9

an alkene group, while the band at 1313 cm^{-1} is indicative of C–N stretching of amines. Furthermore, the C–O stretching vibrations associated with esters and carboxylic functional groups can be identified between the ranges of 1000 and 1300 cm^{-1}. Lastly, the distinct sharp bands observed at 491 cm^{-1} and 435 cm^{-1} are representative of the Zn–O stretching bands[46, 47].

3.2 Local anesthetic activity

3.2.1 Effect of ZnO NPs on hot-plate test

Data from the hot-plate test indicated that a dosage of 2.5 mg/kg ZnO NPs didn't significantly change the anti-pain response, but there was an observable trend towards increased ZnO NPs in mice tested on the hot-plate. On the other hand, ZnO NPs doses ranging from 5-20 mg/kg, when administered orally, induced a noticeable dose-dependent pain relief effect 30 min to post-injection. The pain relief effect (MPE%) observed with 20 mg/kg ZnO NPs was (34.21 ± 7.2) %, which closely mirrored the effect of morphine at (32.12 ± 2.2) %. In contrast, the vehicle administration exhibited no pain-relieving effects (Fig. 5).

3.2.2 Effect of ZnO NPs on acetic acid induced writhing response

Table 1 demonstrated that a smaller dosage of ZnO NPs (2.5 mg/kg) indicated a potential reduction in writhing counts over 20 minutes. However, when compared to the Control group, these results were not statistically significant. At 5 mg/kg of ZnO NPs, notable reduced writhing episodes triggered by the intraperitoneal acetic acid injection in mice was found. Similarly, the positive control, aspirin at 200 mg/kg, markedly decreased the writhing incidents as seen in Table 1. The effects of ZnO NPs were more pronounced at 10 and 20 mg/kg dosages. Yet, there wasn't a considerable distinction among the groups treated with 10 mg/kg and 20 mg/kg of ZnO NPs. In contrast, the vehicle's administration did not yield any pain-relieving effects.

3.2.3 Efficacy of ZnO NPs on formalin-induced hind paw licking response and PGE_2 release

Results, as depicted in Table 2, demonstrate that ZnO NPs, at doses from 2.5 to 10 mg/kg, provided a dose-responsive mitigation of the dual-phase pain reactions (both neurogenic and inflammatory) in mice triggered by formalin. The pain-relieving effects appeared more pronounced during the inflammatory (late) phase than during the neurogenic (early) phase. Concurrently, the weight difference between the left and right paws decreased in a dose-dependent manner, suggesting ZnO NP's potential anti-inflammatory properties. The positive control, aspirin at 200 mg/kg, not only significantly reduced pain reactions across both phases but also mitigated the inflammatory swelling in the mouse paws. In contrast, the vehicle's administration did not exhibit any pain-relieving effects. It's important to

Table 2 Formalin test showing antinociceptive effect of ZnO NPs on the early phase (0-5 min) and the late phase (15-30 min) in mice.

Treatment	Dose (mg/kg)	Licking time (S)		Equation weight of left and right foot (g)
		Early phase 0-5 min	Late phase 15-30 min	
Control	–	91.4 ± 21	96.0 ± 13	0.06 ± 0.02
Asprin	200	58.4 ± 15	48.6 ± 8.5	0.06 ± 0.02
EABR	10	52.0 ± 16	3.7 ± 7.5	0.04 ± 0.01
	5	73.0 ± 26	23.5 ± 5.6	0.05 ± 0.01
	2.5	81.4 ± 32	43.6 ± 4.2	0.06 ± 0.02
	1.0	87.5 ± 23	77.6 ± 5.3	0.06 ± 0.02

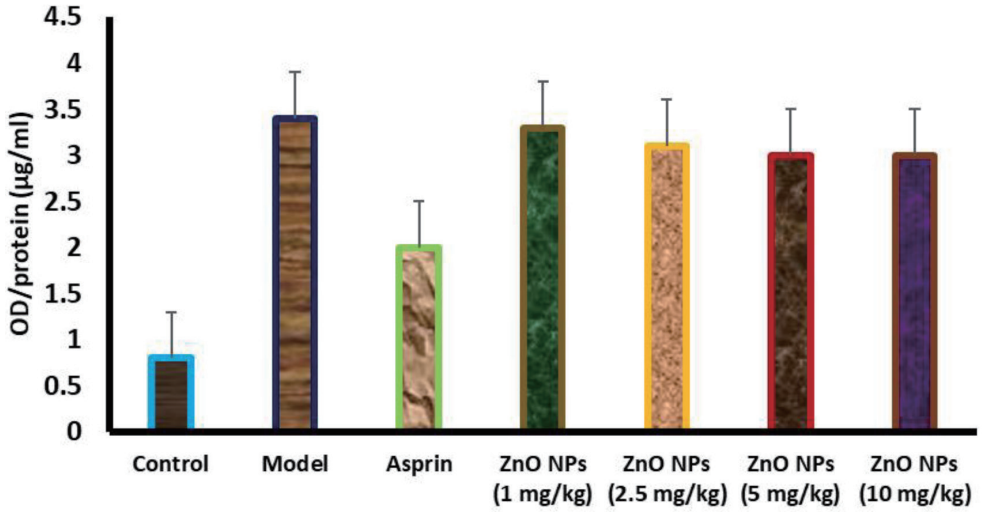

Fig. 6 Effect of ZnO NPs on PGE_2 production in hind paw of mice induced by formalin.

note that a smaller dose of ZnO NPs, 1.0 mg/kg, failed to show a significant effect on pain reactions when compared to the control group.

As illustrated in Fig. 6, formalin induction led to an obvious rise in PGE_2 production in the mouse hind paw, when compared to the baseline control. The positive control drug, aspirin at 200 mg/kg, efficiently curtailed this PGE_2 surge. Nevertheless, the concentrations of ZnO NPs between 1 to 10 mg/mL didn't show any substantial restraint on PGE_2 release. In summary, our research underscores that ZnO NPs exhibits analgesic properties within a narrow therapeutic window. The results suggest the potential of ZnO NPs to be refined and adapted as an efficacious pharmaceutical solution for managing and treating a spectrum of pain conditions, given its appropriate application. It is understood that prepared plant extract mediated ZnO NPs has a possible effect against chronic and acute phases of inflammation not via PGE_2 pathway. However, further indeep studies should be performed to know about exact mechanisms of analgesic activity of prepared ZnO NPs.

3.3 Acute lung injury studies

3.3.1 Administering ZnO NPs orally prior to hydrochloric acid exposure

Figure 7A presents the total cellular content in the BALF obtained from mice subjected to various treatments. It is evident from the data that HCl exposure caused a significant surge in total cellular count when compared to the control group. Intriguingly, pre-treatment with the ZnO NPs brought down this elevated cell count, showcasing a dose-responsive protective effect. The most notable protective effect was discerned at the 200 mg/kg dose.

On the other hand, the results of cellular composition within the BALF, aligned with previous findings: the predominant cellular influx into the lungs post-HCl induced ALI were neutrophils, as shown in Fig. 7B. The HCl introduction intratracheally led to a significant boost in neutrophil numbers relative to the control. However, administering varying ZnO NPs dosages before HCl exposure noticeably curbed this neutrophil influx in a dose-responsive manner. The highest reduction in neutrophil counts was achieved with 200 mg/kg ZnO NPs dose.

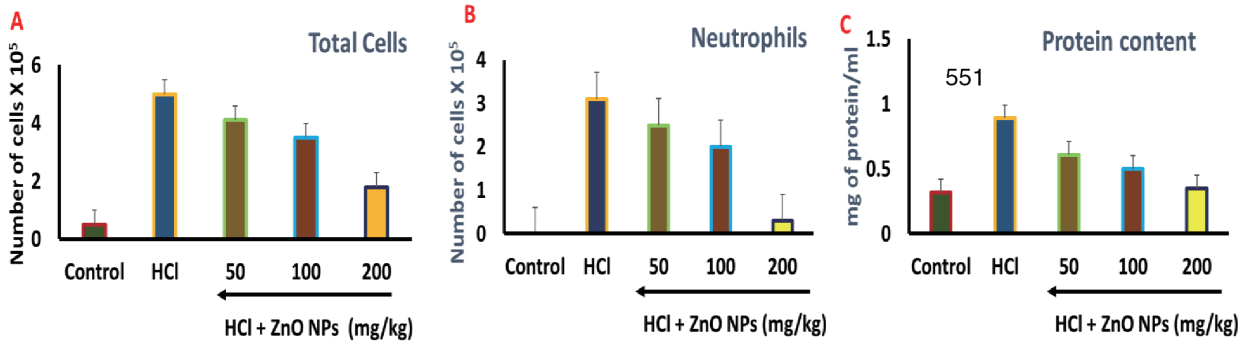

Fig. 7 Levels of Total cells (A) neutrophils (B) and total protein (C) after oral administration of ZnO NPs before HCl treatment.

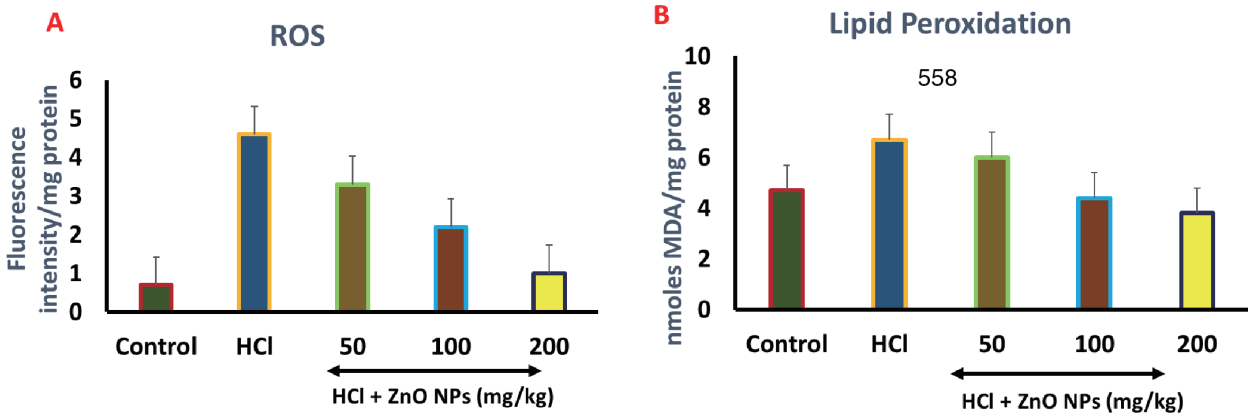

Fig. 8 Effect of ZnO NPs on levels of ROS (A) and lipid peroxidation (B) in lungs on HCl treatment.

ALI's pathology includes the injury of both endothelial and epithelial barriers, resulting in protein-rich fluid accumulation and inflammation instigated by an array of cytokines and chemokines. These inflammatory molecules could emanate from inflammatory cells, lung's own epithelial cells, or even fibroblasts. The endothelial barrier's weakening further facilitates leukocytes' migration into lung tissues, exacerbating pulmonary dysfunction.

To know the degree of pulmonary fluid accumulation, the protein levels in the mice's BALF, were measured (shown in Fig. 7C). HCl exposure triggered a marked upsurge in BALF protein content. Conversely, prior treatment with the ZnO NPs attenuated this protein increase in a dose-responsive manner. The effect of the ZnO NPs in normalizing BALF protein levels was pronounced at doses of both 100 mg/kg and 200 mg/kg. In sum, the gathered evidence robustly indicates the potential therapeutic efficacy of ZnO NPs in counteracting inflammation and fluid accumulation in the lungs following acid aspiration.

3.3.2 Levels of ROS and lipid peroxidation in lungs on HCl treatment

Figure 8A illustrates the variations in ROS concentrations within the lung tissues of mice subjected to various treatments. When mice were exposed to HCl via intratracheal route, there was a marked surge in ROS levels. However, when mice received ZnO NPs orally prior to HCl exposure, there was a systematic reduction in ROS levels, with the most significant decrease observed at a dosage of 200 mg/kg. Figure 8B showed the impact of the ZnO NPs on the MDA levels within the lungs across diverse mouse groups. Upon HCl exposure, the MDA levels in lung samples sharply elevated compared to the standard. Different dosages of the ZnO NPs helped in gradually normalizing the MDA levels. The most pronounced effect was seen at a dosage of 200 mg/kg.

3.3.3 Levels of glutathione content and catalase activity in lungs upon HCl treatment

During oxidative stress process, GSH, in its reduced state, undergoes oxidation to form Glutathione disulfide (GSSG). Consequently, the reversion of GSSG to its reduced state becomes impaired. This reduction in GSH levels is often utilized as key for oxidative stress. Catalase is suggested to contribute to intracellular antioxidant defence strategies by curbing the accumulation of H_2O_2[48, 49]. To assess the ZnO NP's efficacy in ameliorating these metrics post-HCl exposure, both GSH concentration and catalase function were quantified. As illustrated in Fig. 9A, there was a notable decline in GSH concentration after HCl exposure. Administering a 50 mg/kg dose of the ZnO NPs exhibited no notable influence on the GSH fluctuation.

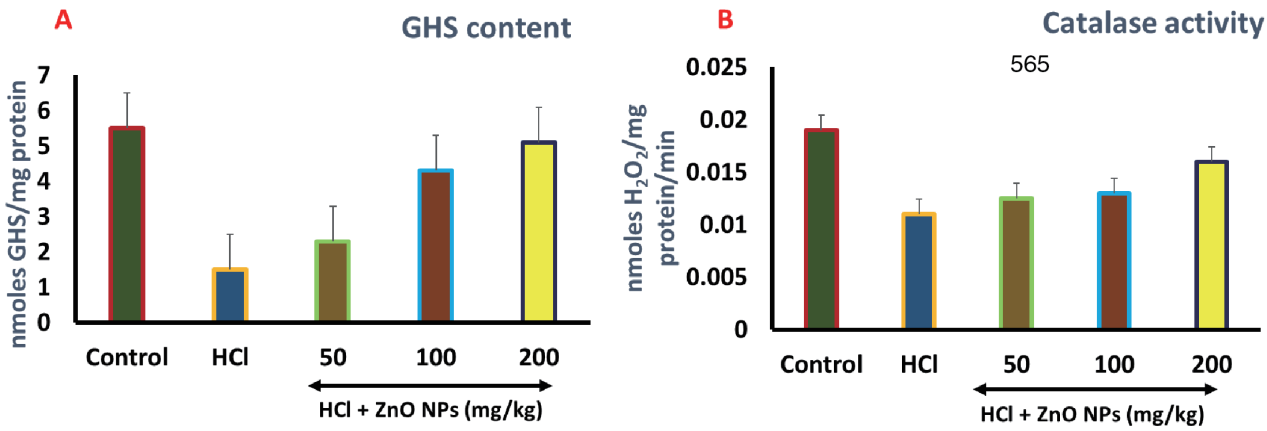

Fig. 9 Effect of ZnO NPs on glutathione levels (A) and Catalase activity (B) in lungs on HCl treatment.

Nevertheless, elevating the ZnO NPs dosage to 100 mg/kg and 200 mg/kg yielded a significant return of GSH concentrations towards baseline levels.

Figure 9B presents the catalytic performance of the catalase enzyme extracted from lung homogenates of varied mouse cohorts. Following the intratracheal introduction of HCl, a significant reduction in catalase functionality was observed. Prophylactic administration of the ZnO NPs, especially at a concentration of 200 mg/kg, significantly ameliorated the catalase function. Conversely, lesser concentrations of the ZnO NPs exhibited negligible alterations in catalase performance in juxtaposition with the HCl-exposed cohort.

4 Conclusions

In conclusion, ZnO NPs were prepared using *Ottonia anisum* leaf extract as reducing and stabilizing agent. XRD and HR-TEM, confirmed the existence of agglomerated ZnO NPs with an average diameter of 40 nm. Further, nociceptive studies revealed that ZnO NPs exerted a dose-dependent analgesic effect in both the hot-plate and the acetic acid-induced writhing tests. Moreover, ZnO NPs exhibited a notable reduction in pain responses during both the initial and subsequent phases of the formalin test, without any change in PGE_2 production in mice. On the other hand, acute lung injury studies revealed that the administration of ZnO NPs decreased the neutrophil infiltration into the lungs in a dose-responsive manner. Additionally, the ZnO NPs appeared to recalibrate the lung's redox equilibrium following HCl exposure. All these results further indicated the potential of biofabricated ZnO NPs for future applications in analgesics and acute lung injury treatments.

Authors Contributions

Guiqin Fan: Manuscript writing, Experimental work. Jing Yu: Manuscript writing, Experimental work. Zhengzheng Tao: Experimental work, Literature survey. Xingjia Qian: Literature survey, Data analysis. Qinghong Qian: Manuscript writing, Experimental work. Jun Shu: Experimental work, Literature survey. Dongfang Shi: Experimental work, Data analysis. Luhong Shen: Experimental work, Data analysis. Bing Lu: Supervision, Manuscript drafting, Literature survey, Data analysis. Hong Lv: Data analysis, Experimental support.

Funding

Authors declared that no funding was associated with this work.

Acknowledgements

Authors are thankful to Taicang Hospital of Traditional Chinese Medicine for providing platform to do this research.

Data Availability

The data associated with the findings of this study are available from the corresponding authors, [Bing Lu], upon reasonable request.

Disclosure of Interest

The authors declared no conflict of interest related to this work.

References

1) Ramsden, J. *Nanotechnology: An Introduction*, William Andrew(2016).
2) Albrecht, M.A.; Evans, C.W; Raston, C.L. Green chemistry and the health implications of nanoparticles. *Green Chem.* **8**, 417-432(2006).
3) Herlekar, M.; Barve, S; Kumar, R. Plant-mediated green synthesis of iron nanoparticles. *J. Nanopart.* **2014**, 140614(2014).
4) Simonis, F; Schilthuizen, S. *Nanotechnology; Innovation Opportunities for Tomorrow's Defence*. TNO Science & Industry Future Technology Center, The Netherlands(2006).
5) Iravani, S. Green synthesis of metal nanoparticles using plants. *Green Chem.* **13**, 2638-2650(2011).
6) Duan, H.; Wang, D; Li, Y. Green chemistry for nanoparticle synthesis. *Chem. Soc. Rev.* **44**, 5778-5792(2015).
7) Bala, N.; Saha, S.; Chakraborty, M.; Maiti, M.; Das, S. *et al.* Green synthesis of zinc oxide nanoparticles using *Hibiscus subdariffa* leaf extract: Effect of temperature on synthesis, anti-bacterial activity and anti-diabetic activity. *RSC Adv.* **5**, 4993-5003(2015).
8) Hasan, S.A. Review on nanoparticles: Their synthesis and types. *Res. J. Recent Sci.* **4**, 1-3(2015).
9) Barzinjy, A.A.; Hamad, S.M.; Aydın, S.; Ahmed, M.H; Hussain, F.H. Green and eco-friendly synthesis of nickel oxide nanoparticles and its photocatalytic activity for methyl orange degradation. *J. Mater. Sci. Mater. Electron.* **31**, 11303-11316(2020).
10) Altavilla, C; Ciliberto, E. in *Inorganic Nanoparticles: Synthesis, Applications, and Perspectives. An Overview*(Altavilla, C.; Ciliberto, E. eds.), CRC Press, New York, pp 1-17(2011).
11) Al-Naamani, L.; Dobretsov, S; Dutta, J. Chitosan-zinc oxide nanoparticle composite coating for active food packaging applications. *Innov. Food Sci. Emerg. Technol.* **38**, 231-237(2016).
12) Sankapal, B.R.; Gajare, H.B.; Karade, S.S.; Salunkhe, R.R; Dubal, D.P. Zinc oxide encapsulated carbon nanotube thin films for energy storage applications. *Electrochim. Acta* **192**, 377-384(2016).
13) Kumar, R.; Al-Dossary, O.; Kumar, G; Umar, A. Zinc oxide nanostructures for NO_2 gas–sensor applications: A review. *Nano-Micro Lett.* **7**, 97-120(2015),
14) Kumar, S.G; and Rao, K.K. Zinc oxide based photocatalysis: Tailoring surface-bulk structure and related interfacial charge carrier dynamics for better environmental applications. *RSC Adv.* **5**, 3306-3351(2015).
15) Hatamie, A.; Khan, A.; Golabi, M.; Turner, A.P.; Beni, V. *et al.* Zinc oxide nanostructure-modified textile and its application to biosensing, photocatalysis, and as antibacterial material. *Langmuir* **31**, 10913-10921 (2015),
16) Mishra, P.K.; Mishra, H.; Ekielski, A.; Talegaonkar, S; Vaidya, B. Zinc oxide nanoparticles: A promising nanomaterial for biomedical applications. *Drug Discovery Today* **22**, 1825-1834(2017).
17) Nagajyothi, P.; Cha, S.J.; Yang, I.J.; Sreekanth, T.; Kim, K.J; Shin, H.M. Antioxidant and anti-inflammatory activities of zinc oxide nanoparticles synthesized using *Polygala tenuifolia* root extract. *J. Photochem. Photobiol. B* **146**, 10-17(2015).
18) Cai, X.; Luo, Y.; Zhang, W.; Du, D; Lin, Y. pH-Sensitive ZnO quantum dots–doxorubicin nanoparticles for lung cancer targeted drug delivery. *ACS Appl. Mater. Interfaces* **8**, 22442-22450(2016).
19) Gutha, Y.; Pathak, J.L.; Zhang, W.; Zhang, Y; Jiao, X. Antibacterial and wound healing properties of chitosan/poly(vinyl alcohol)/zinc oxide beads(CS/PVA/ZnO). *Int. J. Biol. Macromol.* **103**, 234-241(2017).
20) Lai, L.; Zhao, C.; Su, M.; Li, X.; Liu, X. *et al. In vivo* target bio-imaging of Alzheimer's disease by fluorescent zinc oxide nanoclusters. *Biomater. Sci.* **4**, 1085-1091(2016).
21) Lammers, T.; Sofias, A.M.; van der Meel, R.; Schiffelers, R.; Gert, S. *et al.* Dexamethasone nanomedicines for COVID-22. *Nat. Nanotechnol.* **15**, 622-624(2020).
22) Zhang, P.; Zhang, Y.; Ding, X.; Shen, W.; Li, M. *et al.* A multistage cooperative nanoplatform enables intracellular co-delivery of proteins and chemotherapeutics for cancer therapy. *Adv. Mater.* **32**, e2000013(2020).
23) Li, J.; Jia, Y.; Zhang, P.; Yang, H.; Cong, X. *et al.* Celastrol self-stabilized nanoparticles for effective treatment of melanoma. *Int. J. Nanomedicine* **15**, 1205-1214(2020).
24) de Oliveira, M.T.P.; de Sa Coutinho, D.; Tenorio de Souza, E.; Stanisçuaski Guterres, S.; Pohlmann, A.R. *et al.* Orally delivered resveratrol-loaded lipid-core nanocapsules ameliorate LPS-induced acute lung injury via the ERK and PI3K/Akt pathways. *Int. J. Nanomedicine* **14**, 5215-5228(2019).
25) Zhang, C.Y.; Lin, W.; Gao, J.; Shi, X.; Davaritouchaee, M. *et al.* pH-Responsive nanoparticles targeted to lungs for improved therapy of acute lung inflammation/injury. *ACS Appl. Mater. Interfaces* **11**, 16380-16390 (2019).
26) Jin, F.; Liu, D.; Yu, H.; Qi, J.; You, Y. *et al.* Sialic acid-functionalized PEG-PLGA microspheres loading mitochondrial-targeting-modified curcumin for acute lung injury therapy. *Mol. Pharm.* **16**, 71-85(2019).
27) Wang, M.; Wang, K.; Deng, G.; Li, X.; Wu, X. *et al.* Mitochondria-modulating porous $Se@SiO_2$ nanoparticles provide resistance to oxidative injury in airway epithelial cells: Implications for acute lung injury. *Int. J. Nanomedicine* **15**, 2287-2302(2020).
28) Wang, L.; Zhang, H.; Sun, L.; Gao, W.; Xiong, Y. *et al.* Manipulation of macrophage polarization by peptide-coated gold nanoparticles and its protective effects on

acute lung injury. *J. Nanobiotechnology* **18**, 38 (2020).
29) Dos Santos Haupenthal, D.P.; Mendes, C.; de Bem Silveira, G.; Zaccaron, R.P.; Corrêa, M.E.A.B. *et al.* Effects of treatment with gold nanoparticles in a model of acute pulmonary inflammation induced by lipopolysaccharide. *J. Biomed. Mater. Res. A* **108**, 103-115 (2020).
30) Gao, W.; Wang, Y.; Xiong, Y.; Sun, L.; Wang, L. *et al.* Size-dependent anti-inflammatory activity of a peptide-gold nanoparticle hybrid *in vitro* and in a mouse model of acute lung injury. *Acta Biomater.* **85**, 203-217(2019).
31) Yu. H.P.; Liu, F.C.; Umoro, A.; Lin, Z.C.; Elzoghby, A.O. *et al.* Oleic acid-based nanosystems for mitigating acute respiratory distress syndrome in mice through neutrophil suppression: how the particulate size affects therapeutic efficiency. *J. Nanobiotechnology* **18**, 25(2020).
32) Okeke, E.B.; Louttit, C.; Fry, C.; Najafabadi, A.H.; Han, K. *et al.* Inhibition of neutrophil elastase prevents neutrophil extracellular trap formation and rescues mice from endotoxic shock. *Biomaterials* **238**, 119836 (2020).
33) Liu, F.C.; Yu, H.P.; Lin, C.Y.; Elzoghby, A.O.; Hwang, T.L; Fang, J.Y. Use of cilomilast-loaded phosphatiosomes to suppress neutrophilic inflammation for attenuating acute lung injury: The effect of nanovesicular surface charge. *J. Nanobiotechnology* **16**, 35(2018).
34) Jiang, S.; Li, S.; Hu, J.; Xu, X.; Wang, X. *et al.* Combined delivery of angiopoietin-1 gene and simvastatin mediated by anti-intercellular adhesion molecule-1 antibody-conjugated ternary nanoparticles for acute lung injury therapy. *Nanomedicine* **15**, 25-36(2019).
35) Ge, C.; Yang, J.; Duan, S.; Liu, Y.; Meng, F; Yin, L. Fluorinated alpha-helical polypeptides synchronize mucus permeation and cell penetration toward highly efficient pulmonary siRNA delivery against acute lung injury. *Nano Lett.* **20**, 1738-1746(2020).
36) Piao, C.; Zhuang, C.; Choi, M.; Ha, J; Lee, M. A RAGE-antagonist peptide potentiates polymeric micelle-mediated intracellular delivery of plasmid DNA for acute lung injury gene therapy. *Nanoscale* **12**, 13606-13617 (2020).
37) Lowry, O.H.; Rosebrough, N.J.; Farr, A.L; Randall, R.J. Protein measurement with the folin phenol reagent. *J. Biol. Chem.* **193**, 265-75(1951).
38) Wang, H; Joseph, J.A. Quantifying cellular oxidative stress by dichlorofluorescein assay using microplate reader. *Free Radic. Biol. Med.* **27**, 612-616(1999).
39) Ohkawa, H.; Ohishi, N; Yagi, K. Assay for lipid peroxides in animal tissues by thiobarbituric acid reaction. *Anal. Biochem.* **95**, 351-358(1979).
40) Ellman, G.L. Tissue sulfhydryl groups. *Arch. Biochem. Biophys.* **82**, 70-77(1959).
41) Zahler, W.L; Cleland, W.W. A specific and sensitive assay for disulfides. *J. Biol. Chem.* **243**, 716-719(1968).
42) Aebi, H. Catalase *in vitro*. *Methods Enzymol.* **105**, 121-126(1984).
43) Sasani Ghamsari, M.; Alamdari, S.; Han, W; Park, H. Impact of nanostructured thin ZnO film in ultraviolet protection. *Int. J. Nanomed.* **12**, 207-216(2016).
44) Tan, S.T.; Chen, B.J.; Sun, X.W.; Fan, W.J.; Kwok, H.S. *et al.* Blueshift of optical band gap in ZnO thin films grown by metal-organic chemicalvapor deposition. *J. Appl. Phys.* **98**, 013505(2005).
45) Debanath, M.K; Karmakar, S. Study of blueshift of optical band gap in zinc oxide(ZnO)nanoparticles prepared by low-temperature wet chemical method. *Mater. Lett.* **11**, 116-119(2013).
46) Chen, C.; Yu, B.; Liu, P.; Liu, J; Wang, L. Investigation of nano-sized ZnO particles fabricated by various synthesis routes. *J. Ceram. Process. Res.* **12**, 420-425 (2011).
47) Lu, J.; Batjikh, I.; Hurh, J.; Han, Y.; Ali, H. *et al.* Photocatalytic degradation of methylene blue using biosynthesized zinc oxide nanoparticles from bark extract of *Kalopanax septemlobus*. *Optik* **182**, 980-985(2019).
48) Comhair, S.A; Erzurum, S.C. Antioxidant responses to oxidant-mediated lung diseases. *Am. J. Physiol. Lung Cell. Mol. Physiol.* **283**, L246-55(2002).
49) Birben, E.; Sahiner, U.M.; Sackesen, C.; Erzurum, S; Kalayci, O. Oxidative stress and antioxidant defense. *World Allergy Organ. J.* **5**, 9-19(2012).